Article

Microsecond All-Optical Modulation by Biofunctionalized Porous Silicon Microcavity

Dániel Petrovszki , Sándor Valkai , Lóránd Kelemen , László Nagy , Vivechana Agarwal , Szilvia Krekic , László Zimányi * , András Dér *

Posted Date: 21 June 2023

doi: 10.20944/preprints202306.1497.v1

Keywords: porous silicon; photoactive yellow protein; photocycle; optical modulation

Article

Microsecond All-Optical Modulation by Biofunctionalized Porous Silicon Microcavity

Dániel Petrovszki [1,4], Sándor Valkai [1], Lóránd Kelemen [1], László Nagy [2,5], Vivechana Agarwal [3], Szilvia Krekic [1,4], László Zimányi [1,*], András Dér [1,*]

[1] Institute of Biophysics, Biological Research Centre, Eötvös Loránd Research Network, 6726 Szeged, Hugary
danielpetrovszki37@gmail.com (D.P.); valkai.sandor@brc.hu (S.V.); zimanyi.laszlo@brc.hu (L.Z.); kelemen.lorand@brc.hu (L.K.); krekic.szilvia@brc.hu (S.K.); der.andras@brc.hu (A.D.)

[2] Department of Medical Physics and Informatics, Faculty of Science and Informatics, Albert Szent-Györgyi Medical School, University of Szeged, 6720 Szeged, Hungary
L.Nagy@physx.u-szeged.hu (L.N.)

[3] Centro de Investigación en Ingeniería y Ciencias Aplicadas-IICBA, Universidad Autónoma del Estado de Morelos, Cuernavaca, Morelos, 62209, Mexico
vagarwal@uaem.mx (V.A.)

[4] Doctoral School of Multidisciplinary Medical Science, University of Szeged, 6720 Szeged, Hungary

[5] Institute of Plant Biology, Biological Research Centre, Eötvös Loránd Research Network, 6726 Szeged, Hugary

* Correspondence: zimanyi.laszlo@brc.hu, der.andras@brc.hu

Abstract: We successfully created a composite photonic structure out of porous silicon (PSi) microcavities doped by the photochromic protein, photoactive yellow protein (PYP). Massive incorporation of the protein molecules into the pores was substantiated by a 30-nm shift of the resonance dip upon functionalization, and light-induced reflectance changes of the device due to the protein photocycle were recorded. Model calculations for the photonic properties of the device were consistent with earlier results on the nonlinear optical properties of the protein, whose degree of incorporation into the PSi structure was also estimated. The successful proof-of-concept results are discussed in light of possible practical applications in the future.

Keywords: porous silicon; photoactive yellow protein; photocycle; optical modulation

1. Introduction

1.1. Optical switching by chromoproteins

The nonlinear optical (NLO) properties of dried chromoprotein samples have recently been intensively investigated for their possible applications as NLO materials in integrated optical devices [1–8]. Most of the potential applications have been envisioned using bacteriorhodopsin- (bR-) based films, as they undergo high refractive index changes (up to $5*10^{-3}$) upon photoexcitation [1–3,9], at the same time showing high cyclicity (> 10^6) and considerable long-term stability [10–12].

More recently, dried samples from other chromoproteins, most notably photoactive yellow protein (PYP), have also been proven to possess NLO properties making them suitable for use as NLO materials in future integrated optics applications [13–16]. PYP films at high enough relative humidity (> 60 %) preserve the basic scheme of their native photocycle (Figure 1), a series of first-order reactions of metastable conformational states, including intermediates of red- (pR) and blue-shifted (pB) absorption spectra, as compared to that of the resting state (pG). A special advantage of PYP compared to bR resides in its relatively small dimension, water-solubility and, hence, potential of possible incorporation into porous matrices compatible with integrated optics.

Preprints (www.preprints.org) | NOT PEER-REVIEWED | Posted: 21 June 2023 doi:10.20944/preprints202306.1497.v1

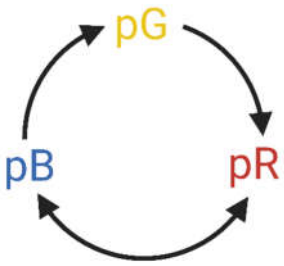

Figure 1. Simplified scheme of the photoactive yellow protein (PYP) photocycle with the resting state (pG) and intermediates of red- and blue- shifted (pR and pB) absorption spectra. The arrows indicate the direction of the photocycle, while the back-and-forth arrow indicates an equilibrium reaction between pB and pR. The figure was created with BioRender.com.

1.2. Porous silicon structures

Porous silicon (PSi) technology allows a facile preparation technique for synthesizing 1D photonic structures with special NLO properties. During the recent years, several proteins have been successfully incorporated into PSi microcavities, for potential applications in bioelectronics, such as in biosensorics or photovoltaics [17–20]. The proteins embedded in the micropores of the PSi structures were shown to preserve their basic functionalities, occasionally with enhanced properties for special applications [21].

1.3. Aim of the study

Here, we report on creating a hybrid photonic structure, a PSi microcavity doped with the soluble chromoprotein PYP, characterizing its static and light-induced dynamic spectral properties, and discussing the main implications of the results for possible biophotonic applications.

2. Materials and Methods

2.1. PYP Sample Preparation

The PYP solution preparation followed the process, previously described in numerous studies of our research group [14,15,22], however, the functionalization protocol for the protein-solid interface was adapted to the PSi substrate.

To promote microcavity infiltration with the protein sample, previously fabricated porous silicon substrates with microcavities were exposed to oxygen plasma at 400 mtorr pressure (@29.6 W RF power) for 60 s (PDC-002 Expanded Plasma Cleaner, Harrick Plasma, Ithaca, NY, USA) hydrophilizing their surfaces. Then, the PYP solution was pipetted on the substrates to fill these cavities. The protein films were left drying for 24 hours on the substrates. Finally, the extra volumes of the PYP coatings on the slides were washed mildly by deionized water (MilliQ water, Synergy® UV Water Purification System, Merck-Millipore, Burlington, MA, USA), and the PYP functionalized porous silicon microcavity samples became ready-to-use for the measurements.

2.2. Porous silicon microcavity (PSiMc) fabrication

PSiMc-s were prepared in dark by a wet electrochemical etching process of highly boron-doped p-type silicon wafers sliced in the (100) crystallographic orientation. Their thickness was in the 500−550 μm range and the specific resistivity in the 0.002−0.004 Ωcm range. The electrolyte for etching was a mixture of hydrofluoric acid (48 wt%), ethanol (98%), and glycerol (98%) in a volumetric ratio of 3:7:1. Freshly etched samples were washed with ethanol and dried with pentane. Etching was performed with a current density of 80 mA/cm^2 (H for high porosity, yielding low effective dielectric constant, n_L) and 40 mA/cm^2 (L for low porosity, yielding high effective dielectroc constant, n_H) [23,24]. The anodization times were set to produce microcavity structures (or Fabry-Perot dielectric filters) of alternating quarter wave layers with d_H and d_L thickness ($n_H d_H = n_L d_L = \lambda/4$ with the

Preprints (www.preprints.org) | NOT PEER-REVIEWED | Posted: 21 June 2023 doi:10.20944/preprints202306.1497.v1

wavelength around 645 nm) in the following sequence: [HL]x5 [**HH]** [LH]x5. The top layer was of high porosity, allowing easy incorporation of PYP macromolecules. The two highly porous layers in the middle (marked by bold face characters), function as an optical cavity with an optical mode corresponding to $\lambda/2$ optical thickness (λ = 645 nm) [20].

2.3. Scanning electron microscopy

Scanning electron microscopic (SEM) images were taken of the PSiMc samples to examine the fine structures both from the top and from the cross-section. The SEM images were taken in high vacuum mode of the instrument (JEOL JSM-7100F-LV, JEOL Corporation, Japan) without metal coating of the PSi surface. The accelerating voltage was set to 15 kV for better resolution but when imaging the layer's cross section, 5 kV acceleration often resulted in images of higher contrast.

2.4. Experimental Setup

2.4.1. PYP infiltrated PSiMc reflectance measurements

The reflectance spectra of the silicon wafers were measured in a direct way. The collimated light of a halogen bulb (70 W, 12 V) illuminated one input of a specific 3 bundle lightguide whose output approached the sample surface to ~ 1 mm distance, perpendicularly. The reflected light was collected by the same bundle and the corresponding output (reflected) light was deflected by a prism into a fiber optic. The fiber optic was led into a miniature spectrometer (Scanspec UV/Vis spectrometer, Scansci Ltd., Vila Nova de Gaia, Portugal), controlled by a PC. The schematics of the setup is shown in the following figure (Figure 2).

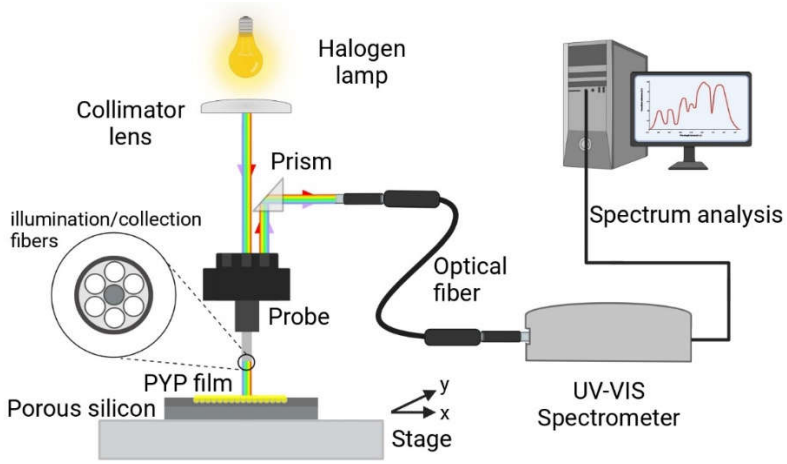

Figure 2. Schematic illustration of the experimental setup for the reflectance measurements of untreated and PYP treated PSiMc samples. The figure was created with BioRender.com.

The reflectance spectra of the PSiMc before and after the infiltration by PYP were measured relative to a reference intensity spectrum measured on the Si wafer outside of the porous area. The micrometric X-Y stage allowed to register the reflectance spectrum at several reproducible positions over the porous area before and after PYP infiltration.

From the shifted reflectance spectrum, it could be determined at what wavelength regime the highest modulation can be expected due to the refractive index change upon excitation of the PYP molecules in the porous silicone layers, hence, the wavelength of the probe beam could be selected (see next section).

2.4.2. Photoinduced all-optical modulation

The all-optical modulation by the PYP-filled PSiMc-s was based on the photoreaction cycle of PYP (Figure 1). To characterize its kinetics, a time-resolved reflectance measurement setup was

Preprints (www.preprints.org) | NOT PEER-REVIEWED | Posted: 21 June 2023 doi:10.20944/preprints202306.1497.v1

designed (Figure 3). In this optical system a Nd:YAG laser (Continuum Surelite II, Amplitude Laser Inc., Milpitas, CA, USA) extended with an optical parametric oscillator (Surelite OPO, Amplitude Laser Inc., Milpitas, CA. 95035, USA) was used as a pump source. The probe beam was a continuous red-light (λ = 675 nm) laser directed perpendicularly on the sample. The pulse energy of the pump was 26 mJ (7 ns pulsewidth, 1.43 Hz), and its wavelength was tuned to 460 nm for exciting the resting state of PYP. The spatial overlapping of the corresponding beams on the sample was achieved by mirrors and an iris diaphragm. The laser power on the sample for the probe was 14.64 mW/cm^2. The angle difference of the probe beam was ~6.6° relative to the pump. The beam diameters at the beam waist were 2 mm for both beams. The PYP-functionalized porous silicon microcavity sample was placed on a motorized stage with a micropositioner (DC-3 K, Märzhäuser Wetzlar GmbH & Co. KG, Wetzlar, Germany) to obtain precise and reproducible illumination location over the porous area. The light reflected from the sample was directed to a photomultiplier (PMT, H5783-01, Hamamatsu, Japan), through a bandpath filter, thus only the probe light could enter the entrance window. The PMT output signal was transmitted to a digital oscilloscope (LeCroy 9310-L, LeCroy, Chestnut Ridge, NY, USA), and then it was processed by a computer. The signal acquisition was triggered by a photodiode hit by the pulse of the pump laser. To record fast kinetics (see section 3.2.) 150 traces, for slow kinetic experiments 400 traces, respectively, were averaged.

To control the relative humidity (RH) of the PYP biofilm, the sample, along with optical accessories and the PMT, was placed in an isolated chamber (Figure 3). The RH was adjusted with supersaturated potassium chloride solution at fixed temperature (78 %, 25 °C) [4]. To maintain the temperature and RH during the measurements, these parameters were continuously monitored with a digital hygro-thermometer (8709 Thermo-Hygrometer, Carl Roth GmbH & Co. KG, Karlsruhe, Germany).

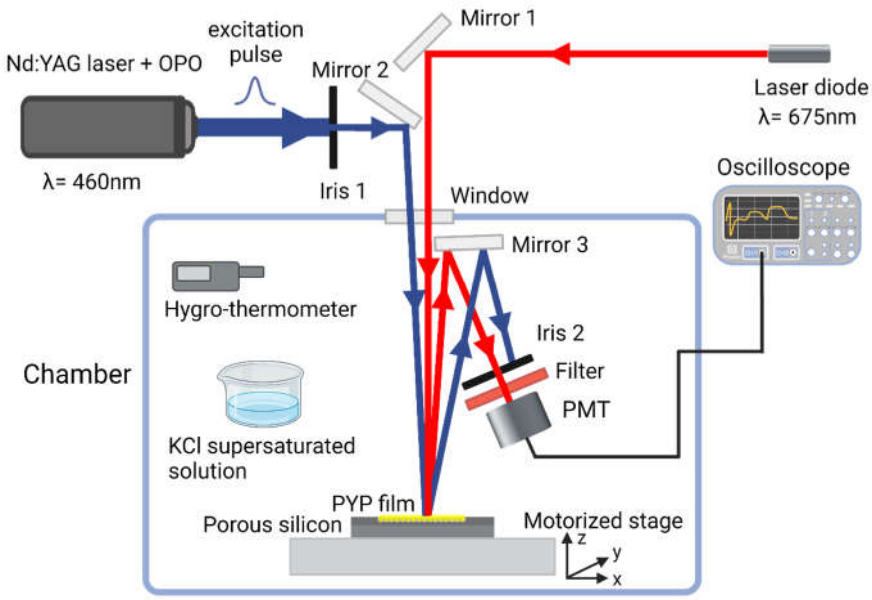

Figure 3. Schematic illustration of the experimental setup used for measurements of PYP-based all-optical modulation. The PYP-functionalized porous silicon sample was placed in an isolated chamber, where the relative humidity was set and monitored. The protein film was illuminated by a blue light pulse (λ = 460 nm) from a Nd:YAG laser with an OPO extension, and probed with continuous red light of a laser diode (λ = 675 nm). The reflected light was filtered and then coupled to a photomultiplier tube (PMT). The signal was transmitted to a digital oscilloscope and processed. The figure was created with BioRender.com.

Preprints (www.preprints.org) | NOT PEER-REVIEWED | Posted: 21 June 2023 doi:10.20944/preprints202306.1497.v1

3. Results and Discussion

3.1. Structure of the PSi microcavity multilayer

In Figure 4a a cross section of the entire multilayer structure is shown. The darker layers correspond to the high porosity regions where the nanopores have thinner walls, whereas the lighter layers correspond to low porosity (thicker pore walls). In Figure 4b the top view of several layers is seen after they became visible due to the partial peeling off of the top layer(s). It offers an excellent view of the internal porous structure of the multilayered structure, showing that the average pore diameter for the high porosity layers is in the range of 100 nm.

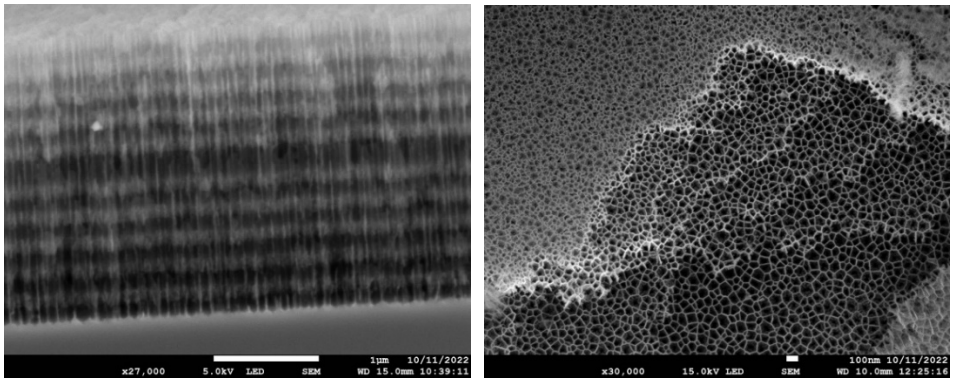

a) **b)**

Figure 4: Scanning electron microscopy images of the porous silicon microcavity samples. a) Cross-sectional view and b) top-view with layer structures

3.2. PYP-functionalization of PSiMcs

To characterize the optical properties of the microcavities, reflectance spectra of the untreated and PYP infiltrated PSiMcs were recorded in the 400-800 nm range. Both reflectance curves (Figure 5) show major resonances corresponding to low-reflectance ('negative') peaks in the red wavelength regime (between 600 and 700 nm). Their shape and the location are characteristic to the porous silicon microcavities. A spectral shift was observed between the reflectance spectra of the untreated and bio-functionalized microcavities. The peak position of the cavity mode shifted from 645 to 667 nm, corresponding to a 22-nm shift towards longer wavelengths upon functionalization, as a consequence of the increase in the refractive index of the porous silicon layers caused by the infiltration of the PYP protein.

The reflectance spectra of the untreated and PYP-functionalized samples were also simulated as follows. The effective refractive index of the low and high porosity layers, n_{PSi}, was calculated by using the Bruggeman equation [25]:

$$(1-p)\cdot\frac{n_{Si}^2-n_{PSi}^2}{n_{Si}^2+2\cdot n_{PSi}^2}+p\cdot\frac{n_A^2-n_{PSi}^2}{n_A^2+2\cdot n_{PSi}^2}=0 \quad (1)$$

where p is porosity, n_{Si} is the wavelength-dependent refractive index of bulk silicon, and n_A is the refractive index of air, equal to 1, for the non-functionalized sample, whereas

$$n_A=\beta\cdot n_{PYP}+(1-\beta) \quad (2)$$

for the functionalized sample. Here β stands for the volume fraction occupied by the protein in the pores ($0 \le \beta \le 1$) and n_{PYP} was taken as 1.53. Once the refractive indices for the two layer types are calculated with the porosities as input parameters, the reflectance spectrum of the multilayer can be calculated using the transfer matrix formalism [26], taking into account the thickness of the low and high porosity layers as determined from the electron micrographs, such as shown in Figure 4a. Figure

Preprints (www.preprints.org) | NOT PEER-REVIEWED | Posted: 21 June 2023 doi:10.20944/preprints202306.1497.v1

5 shows the calculated spectra based on the above model, with n_A equal to 1 and to 1.042 for the sample before and after functionalization, respectively. The porosities were taken as 0.772 and 0.870 for the low and the high porosity layers, respectively. Except for minor details the calculated spectra reproduce well the measured spectra and, in particular, the spectral shift of the resonance dip as a result of functionalization. From Equation (2) it follows that the protein layer occupies ~8% of the volumes of the pores ($\beta = 0.079$).

Based on these results, we can deduce that infiltration of the protein into the cavities took place, changing the optical properties of the porous silicon microcavities, offering the possibility of protein-based all-optical modulation on these samples.

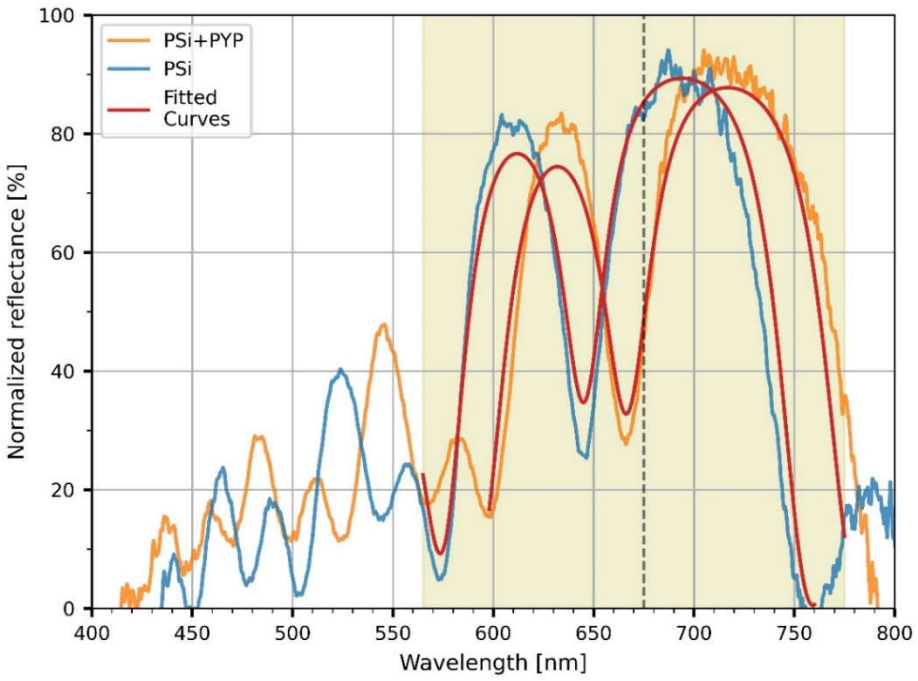

Figure 5. The measured reflectance spectra of porous silicon microcavity (PSiMc) before (blue) and after (orange) functionalization by PYP, and the corresponding calculated spectra based on Equations 1 and 2 (red). For details of the model calculations see text. Thin dashed line represents the wavelength of the probe light at 675 nm for the all-optical modulation experiments.

3.3. Demonstration of all-optical modulation on the biofunctionalized PSiMc samples

Next, we focused on the demonstration of an all-optical modulation by the PYP-infiltrated PSiMc samples. Upon light excitation of PYP at 460 nm, the photoactivation of the protein and the resulting change in the reflectance of the functionalized PSiMc was monitored by using a time-resolved experimental setup. The modulated signals were acquired at two different timescales, 0.5 and 400 ms, respectively. The signals were recorded from the same region of the sample where the reflectance spectra were measured. The wavelength of the probe light beam (675 nm) was chosen to match the steeply changing region of the spectrum beyond the main cavity peak (see Figure 5), in order to sensitively detect any light-induced shift of the resonance spectrum. The intensity changes registered upon light excitation showed complex, bipolar relaxation kinetics, with a fast negative and a slow positive phase (Figure 6). The decrease and successive increase in the intensity of the reflected light is interpreted as a consequence of a rapid red-shift of the reflection spectrum of the sample, followed by a slow blue-shift, respectively, before decaying to the initial level. This row of events is consistent with a rapid formation of the red-shifted pR, and a subsequent accumulation of the blue-shifted pB intermediates, in agreement with the known photocycle of PYP, and the Kramers-Kronig relations [13]. After the fast, unresolved drop of the signal, two exponential components could be fitted to the decay of the negative, and one for the positive phase, with high goodness of fit ($R^2_{fast} = 0.83$, $R^2_{slow} =$

Preprints (www.preprints.org) | NOT PEER-REVIEWED | Posted: 21 June 2023 doi:10.20944/preprints202306.1497.v1

0.88). The time constants of the two negative components at the 0.5 ms timescale were $\tau_1 = 24$ µs and $\tau_2 = 281$ µs (Figure 6b, 6c), while $\tau_3 = 131$ ms for the positive phase registered on the millisecond scale (Figure 6d). The values are close to the ones obtained by evaluating absorption kinetic signals measured earlier under different conditions [13, 27]. The component amplitudes were -0.012 V for the fast signal on a 4 V baseline (Figure 6a), whereas -0.004 V on a 2 V baseline for the slow signal (Figure 6d), resulting in a 0.2-0.3% relative output signal modulation, while the amplitude of noise was 0.001 V. This signal amplitude at 675 nm could be well reproduced by recalculating the reflectance spectra with n_A equal to 1.0421, i.e. a change of 10^{-4} relative to the effective refractive index before light excitation. Taking into account that the contribution by PYP to the effective refractive index of the porous layers corresponds to $\beta = 8\%$, the estimated refractive index change of PYP itself is ~ $5 \cdot 10^{-4}$, in good agreement with our earlier results [13, 14].

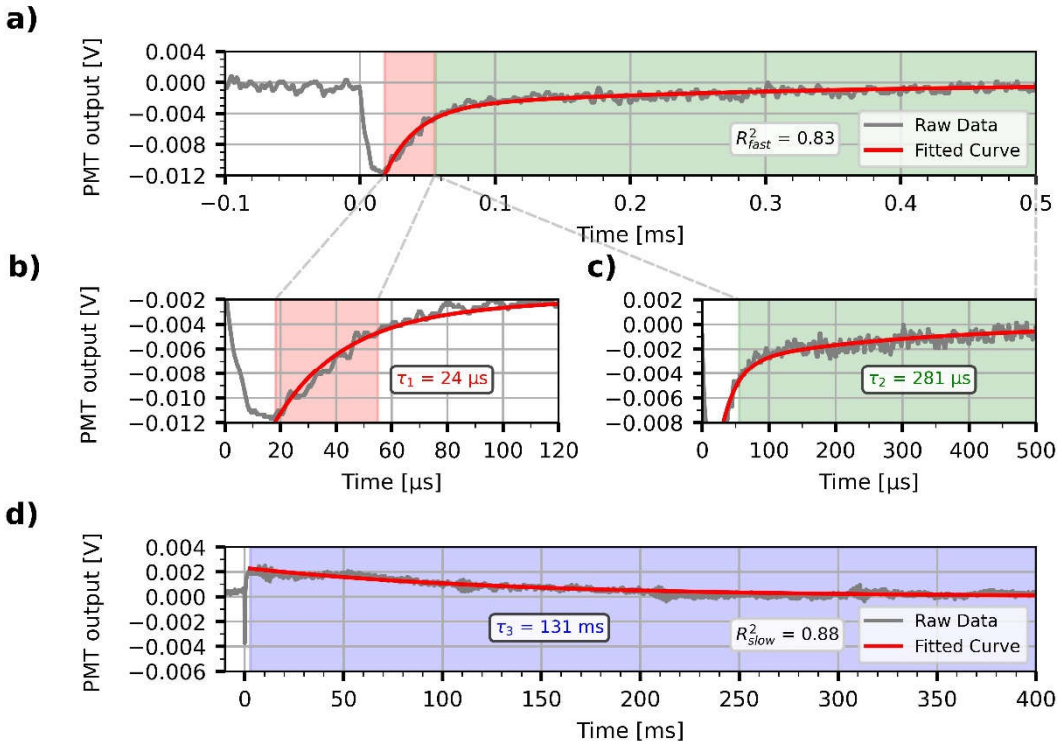

Figure 6. All-optical modulation by PYP-functionalized porous silicon microcavity. For both the fast, negative (**a)**) and the slow, positive (**d)**) phases, the modulation signals followed the reaction kinetics of the photocycle of the protein, with exponential decay time-constants (τ_1, τ_2, τ_3) comparable with those of the PYP photocycle (**b)**, **c)**, **d)**). Exponential components were fitted with high goodness of fit ($R^2_{fast} = 0.83$, $R^2_{slow} = 0.88$).

4. Conclusions and Outlook

The nearly 30-nm shift of the resonance dip upon protein treatment of the porous silicon structure is a clear indication of its successful functionalization by PYP. The size of the shift is also fully consistent with the results of model calculations based on the geometric parameters of the PSi structure and the estimated refractive index of the dried PYP layer. In order to demonstrate light-induced reflectance changes, the probe wavelength of 675 nm was selected by considering that here the protein shows negligible absorption, at the same time, the resonant dip in the reflectance spectrum of the PYP-functionalized PSi has a significant slope. The light-induced traces are consistent with those of absorption kinetic signals of PYP measured under other conditions, and indicative of a successful light-controlled modulation of the reflectance properties of this proof-of-concept protein-doped silicon structure. For its practical application as a composite photonic device, however, the modulation depth of the reflected light has to be considerably improved. This can, in principle, be done by improving the sample-preparation procedure to increase, the presently 8%-efficiency of

protein-doping, or by sharpening the resonance dip of the microcavity, to exploit more efficient all-optical modulation by the same light-induced refractive index change. According to recent results, it is possible to prepare high-Q resonant structures by further increasing the number of [HL] double layers [28], controlling the temperature of anodization [29], or combining PSi structures with layers of porous alumina [30], reaching Q-factors higher than 950 [29]. The recently demonstrated ultrafast refractive index changes of PYP films [16] hold additional possibilities for future photonic applications of such protein-doped PSi materials.

Author Contributions: Conceptualization, A.D., L.N and L.Z.; methodology, V.A., L.K, S.V and L.Z; software, D.P.; validation, D.P., S.V. and A.D.; formal analysis, D.P and L.Z.; investigation, D.P., S.V., L.K, S.K. and A.D; resources, A.D. and L.Z.; data curation, D.P and L.Z.; writing—original draft preparation, D.P., A.D., S.V., L.K.; writing—review and editing, L.N, L.Z., V.A and A.D.; visualization, D.P.; supervision, A.D. and L.Z.; project administration, A.D.; funding acquisition, A.D. and L.Z All authors have read and agreed to the published version of the manuscript.

Funding: National Research and Development Office, Hungary (NKFI-1 K-124922) and Eötvös Loránd Research Network (ELKH KO-36/2021).

Data Availability Statement: The original data are available upon request from the corresponding author.

Conflicts of Interest: The authors declare no conflict of interest or state.

References

1. Ormos, P.; Fábián, L.; Oroszi, L.; Wolff, E.K.; Ramsden, J.J.; Dér, A. Protein-Based Integrated Optical Switching and Modulation. *Appl Phys Lett* **2002**, *80*, 4060–4062, doi:10.1063/1.1481197.
2. Fábián, L.; Wolff, E.K.; Oroszi, L.; Ormos, P.; Dr, A. Fast Integrated Optical Switching by the Protein Bacteriorhodopsin. *Appl Phys Lett* **2010**, *97*, doi:10.1063/1.3462940.
3. Fábián, L.; Heiner, Z.; Mero, M.; Kiss, M.; Wolff, E.K.; Ormos, P.; Osvay, K.; Dér, A. Protein-Based Ultrafast Photonic Switching. *Opt Express* **2011**, *19*, 18861, doi:10.1364/OE.19.018861.
4. Topolancik, J.; Vollmer, F. All-Optical Switching in the near Infrared with Bacteriorhodopsin-Coated Microcavities. *Appl Phys Lett* **2006**, *89*, doi:10.1063/1.2372711.
5. Roy, S.; Sethi, P.; Topolancik, J.; Vollmer, F. All-Optical Reversible Logic Gates with Optically Controlled Bacteriorhodopsin Protein-Coated Microresonators. *Advances in Optical Technologies* **2012**, *2012*, 727206, doi:10.1155/2012/727206.
6. Roy, S.; Prasad, M.; Topolancik, J.; Vollmer, F. All-Optical Switching with Bacteriorhodopsin Protein Coated Microcavities and Its Application to Low Power Computing Circuits. *J Appl Phys* **2010**, *107*, 053115, doi:10.1063/1.3310385.
7. Fábián, L.; Mathesz, A.; Dér, A. New Trends in Biophotonics. *Acta Biologica Szegediensis* 2015, *59*.
8. Topolancik, J.; Vollmer, F. Photoinduced Transformations in Bacteriorhodopsin Membrane Monitored with Optical Microcavities. *Biophys J* **2007**, *92*, 2223–2229, doi:10.1529/biophysj.106.098806.
9. Dér, A.; Valkai, S.; Fábián, L.; Ormos, P.; Ramsden, J.J.; Wolff, E.K. Integrated Optical Switching Based on the Protein Bacteriorhodopsin†. *Photochem Photobiol* **2007**, *83*, 393–396, doi:10.1562/2006-06-21-RA-944.
10. Stuart, J.A.; Marcy, D.L.; Wise, K.J.; Birge, R.R. Volumetric Optical Memory Based on Bacteriorhodopsin. *Synth Met* **2002**, *127*, 3–15, doi:10.1016/S0379-6779(01)00586-0.
11. Hristova, S.G.; Varo, G.; Der, A. Long Time Stability of Purple Membranes from Halobacterium Halobium. *Acta Biochim Biophys Acad Sci Hung* **1984**, *19*.
12. Hampp, N.; Oesterhelt, D. Bacteriorhodopsin and Its Potential in Technical Applications. In *Nanobiotechnology*; Wiley-VCH Verlag GmbH & Co. KGaA: Weinheim, FRG, 2005; pp. 146–167.
13. Krekic, S.; Nagy, D.; Taneva, S.G.; Fábián, · László; László Zimányi, ·; Dér, A. Spectrokinetic Characterization of Photoactive Yellow Protein Films for Integrated Optical Applications. *European Biophysics Journal* **2019**, *48*, 465–473, doi:10.1007/s00249-019-01353-8.
14. Krekic, S.; Zakar, T.; Gombos, Z.; Valkai, S.; Mero, M.; Zimányi, L.; Heiner, Z.; Dér, A. Nonlinear Optical Investigation of Microbial Chromoproteins. *Front Plant Sci* **2020**, *11*, doi:10.3389/fpls.2020.547818.
15. Petrovszki, D.; Krekic, S.; Valkai, S.; Heiner, Z.; Dér, A. All-Optical Switching Demonstrated with Photoactive Yellow Protein Films. *Biosensors (Basel)* **2021**, *11*, 432, doi:10.3390/bios11110432.
16. Krekic, S.; Mero, M.; Dér, A.; Heiner, Z. Ultrafast All-Optical Switching Using Doped Chromoprotein Films. *The Journal of Physical Chemistry C* **2023**, *127*, 1499–1506, doi:10.1021/acs.jpcc.2c06232.

17. Palestino, G.; Martin, M.; Agarwal, V.; Legros, R.; Cloitre, T.; László Zimányi; Gergely, C. Detection and Light Enhancement of Glucose Oxidase Adsorbed on Porous Silicon Microcavities. In Proceedings of the Physica Status Solidi (C) Current Topics in Solid State Physics; 2009; Vol. 6, pp. 1624–1628.
18. Martin, M.; Palestino, G.; Cloitre, T.; Agarwal, V.; Zimányi, L.; Gergely, C. Three-Dimensional Spatial Resolution of the Nonlinear Photoemission from Biofunctionalized Porous Silicon Microcavity. *Appl Phys Lett* **2009**, *94*, 223313, doi:10.1063/1.3148698.
19. Hajdu, K.; Gergely, C.; Martin, M.; Zimányi, L.; Agarwal, V.; Palestino, G.; Hernádi, K.; Németh, Z.; Nagy, L. Light-Harvesting Bio-Nanomaterial Using Porous Silicon and Photosynthetic Reaction Center. *Nanoscale Res Lett* **2012**, *7*, 400, doi:10.1186/1556-276X-7-400.
20. Hajdu, K.; Gergely, C.; Martin, M.; Cloitre, T.; Zimányi, L.; Tenger, K.; Khoroshyy, P.; Palestino, G.; Agarwal, V.; Hernádi, K.; et al. Porous Silicon/Photosynthetic Reaction Center Hybrid Nanostructure. *Langmuir* **2012**, *28*, doi:10.1021/la301888p.
21. Márquez, J.; Cházaro-Ruiz, L.F.; Zimányi, L.; Palestino, G. Immobilization Strategies and Electrochemical Evaluation of Porous Silicon Based Cytochrome c Electrode. *Electrochim Acta* **2014**, *140*, 550–556, doi:10.1016/j.electacta.2014.05.065.
22. Meyer, T.E.; Yakali, E.; Cusanovich, M.A.; Tollin, G. Properties of a Water-Soluble, Yellow Protein Isolated from a Halophilic Phototrophic Bacterium That Has Photochemical Activity Analogous to Sensory Rhodopsin. *Biochemistry* **1987**, *26*, 418–423, doi:10.1021/bi00376a012.
23. Agarwal, V.; del Río, J.A. Tailoring the Photonic Band Gap of a Porous Silicon Dielectric Mirror. *Appl Phys Lett* **2003**, *82*, doi:10.1063/1.1559420.
24. Agarwal, V.; del Río, J.A.; Malpuech, G.; Zamfirescu, M.; Kavokin, A.; Coquillat, D.; Scalbert, D.; Vladimirova, M.; Gil, B. Photon Bloch Oscillations in Porous Silicon Optical Superlattices. *Phys Rev Lett* **2004**, *92*, doi:10.1103/PhysRevLett.92.097401.
25. Bruggeman, D.A.G. Berechnung Verschiedener Physikalischer Konstanten von Heterogenen Substanzen. I. Dielektrizitätskonstanten Und Leitfähigkeiten Der Mischkörper Aus Isotropen Substanzen. *Ann Phys* **1935**, *416*, 636–664, doi:10.1002/andp.19354160705.
26. Born, M.; Wolf, E.; Bhatia, A.B.; Clemmow, P.C.; Gabor, D.; Stokes, A.R.; Taylor, A.M.; Wayman, P.A.; Wilcock, W.L. *Principles of Optics: Electromagnetic Theory of Propagation, Interference and Diffraction of Light*; 7th ed.; Cambridge University Press, 1999; ISBN 9780521642224.
27. Fábián, L., Krekic, S., Tóth-Boconádi, R., Taneva, S.G., Bálint, A.M., Nánai, L., Dér, A., 2017. Integrated optical investigation of two light-sensitive proteins. Presented at the HIGH ENERGY GAMMA-RAY ASTRONOMY: 6th International Meeting on High Energy Gamma-Ray Astronomy, Heidelberg, Germany, p. 040001. https://doi.org/10.1063/1.4972379
28. Zhang, H., Jia, Z., Lv, X., Liu, Y., 2014. Design, analysis and optimization of porous silicon microcavity based on silicon-on-insulator at optical communication wavelengths. Optik 125, 557–560. https://doi.org/10.1016/j.ijleo.2013.07.012
29. Reece, P.J., Lerondel, G., Mulders, J., Zheng, W.H., Gal, M., 2003. Fabrication and tuning of high quality porous silicon microcavities. phys. stat. sol. (a) 197, 321–325. https://doi.org/10.1002/pssa.200306517
30. Cencha, L.G., Antonio Hernández, C., Forzani, L., Urteaga, R., Koropecki, R.R., 2018. Optical performance of hybrid porous silicon–porous alumina multilayers. Journal of Applied Physics 123, 183101. https://doi.org/10.1063/1.5027073